

FURTHER DEVELOPMENT OF AN ALGEBRAIC INTERMITTENCY MODEL FOR SEPARATION-INDUCED TRANSITION UNDER ELEVATED FREE-STREAM TURBULENCE

S. Kubacki¹, D. Simoni², D. Lengani², M. Dellacasagrande², E. Dick³

¹Warsaw University of Technology, Faculty of Power and Aeronautical Engineering, Institute of Aeronautics and Applied Mechanics, Nowowiejska 24, 00-665, Warsaw, Poland;
slawomir.kubacki@pw.edu.pl

²DIME - Università di Genova, Via Montallegro 1, I-16145, Genoa, Italy;
daniele.simoni@unige.it, davide.lengani@edu.unige.it, matteo.dellacasagrande@edu.unige.it

³Ghent University, Fluid Mechanics Research Group, St.-Pietersnieuwstraat 41, 9000, Gent, Belgium; erik.dick@ugent.be

ABSTRACT

A constitutive law for the Reynolds stresses during boundary layer laminar-to-turbulent transition, constructed in previous work by elastic-net regression on an experimental data base, has been incorporated in an algebraic intermittency model. The objective is prediction improvement of transition in a separated layer under an elevated free-stream turbulence level. The modelling for such cases functions through additional production terms in the transport equations of turbulent kinetic energy and specific dissipation rate of a k - ω turbulence model. A sensor detects the front part of a separated layer and activates the production terms. These express the effect of Klebanoff streaks generated upstream of separation on the Kelvin-Helmholtz instability rolls in the separated part of the layer. By the Klebanoff streaks, the breakdown is faster and the speed of breakdown increases by the combined effects of a large adverse pressure gradient and an elevated free-stream turbulence level.

KEYWORDS

LAMINAR-TO-TURBULENT TRANSITION, SEPARATION-INDUCED TRANSITION, BYPASS TRANSITION, ALGEBRAIC TRANSITION MODEL

NOMENCLATURE

| | | | |
|----------|--------------------------------------|----------|---------------------------|
| f_{SS} | shear sheltering factor | S | shear magnitude |
| k | turbulent kinetic energy | Tu | turbulence intensity |
| k_s | small-scale turbulent kinetic energy | γ | intermittency factor |
| k_l | large-scale turbulent kinetic energy | ω | specific dissipation rate |

INTRODUCTION

Accurate prediction of separation of a laminar boundary layer and transition to turbulent state in the separated layer is crucial for analysis and design of turbomachinery components. Without an adequate model for separation-induced transition, the intensity of the breakdown in a separated boundary layer may be seriously underestimated by RANS-based approaches. This may lead to a too large separation bubble with delayed turbulent boundary layer reattachment. Shortcomings of transition models in reproducing the flow characteristics of a separated boundary layer may thus cause a significant lack of quality in the prediction of turbomachinery flows.

The flow within a separated boundary layer depends critically on the Reynolds number, the free-stream turbulence level and the pressure gradient magnitude. Under a low free-stream turbulence level, Kelvin-Helmholtz instability leads to spanwise-oriented vortices, commonly called rolls. They grow while moving downstream and become unstable by spanwise perturbations, which finally cause breakdown and production of turbulence. The turbulent mixing typically results in reattachment of the layer due to increased momentum transfer in the wall-normal direction.

In a laminar boundary layer that separates, but that is perturbed by strong turbulence in the free-stream, Klebanoff streaks form in the attached part of the boundary layer, upstream of separation. The streaks are induced inside the attached laminar layer, due to deep penetration of low-frequency components of perturbations by free-stream fluctuations while high-frequency fluctuations are filtered-out by the boundary layer shear. This low-pass filtering by the laminar layer is called the shear-sheltering effect (Jacobs and Durbin, 2001). When separation occurs, the Klebanoff streaks, produced upstream of separation, interact with the Kelvin-Helmholtz rolls (McAuliffe and Yaras, 2010, Hosseinverdi and Fasel, 2019). Under a low free-stream turbulence level, the rolls cover the full-span of the separated shear layer. But, under a high free-stream turbulence level, the streaks cause splitting of the rolls into part-span rolls. The breakdown process in the separated boundary layer then becomes faster.

A transition model has to take into account the breakdown process in a separated boundary layer for various levels of free-stream turbulence and adverse pressure gradient. The objective of the present work is the improvement of the predictions by a basic transition model, when applied to flows with transition in a separated boundary layer under an adverse pressure gradient and elevated free-stream turbulence. The improvements are relevant for simulations of turbomachinery flows.

THE MODIFIED ALGEBRAIC INTERMITTENCY MODEL

The transport equations of the algebraic intermittency model have the same form as in a previous model version (Kubacki and Dick, 2016). A production term, P_{Kleb} , derived from the elastic-net regression model for Reynolds stresses in transitional flows by Lengani et al. (2020), has been added to the production terms of the turbulent kinetic energy, k , and specific dissipation rate, ω , to model laminar-to-turbulent transition in a separated boundary layer subjected to an elevated turbulence level. The transport equations read:

$$\frac{Dk}{Dt} = \max(\gamma P_k, P_{Kleb}) + P_{KH} - \beta^* k \omega + \frac{\partial}{\partial x_j} \left[\left(\nu + \sigma^* \frac{k}{\omega} \right) \frac{\partial k}{\partial x_j} \right], \quad (1)$$

$$\frac{D\omega}{Dt} = \alpha \frac{\omega}{k} \max(P_k, P_{Kleb}) - \beta \omega^2 + \frac{\partial}{\partial x_j} \left[\left(\nu + \sigma \frac{k}{\omega} \right) \frac{\partial \omega}{\partial x_j} \right] + \frac{\sigma_d}{\omega} \frac{\partial k}{\partial x_j} \frac{\partial \omega}{\partial x_j}. \quad (2)$$

The production terms $P_k = \nu_s S^2$ and P_{KH} are the same as used by Kubacki and Dick (2016). γ is the intermittency variable, ν_s is the small-scale eddy viscosity, which is a part of the total eddy viscosity, and $S = \sqrt{2S_{ij}S_{ij}}$ is the magnitude of the shear rate tensor $S_{ij} = \frac{1}{2}(\partial U_i / \partial x_j + \partial U_j / \partial x_i) - \frac{1}{3}(\partial U_k / \partial x_k) \delta_{ij}$.

The original model functions well for bypass transition in an attached boundary layer by the variables ν_s and γ , and for transition in a separated layer under a low free-stream turbulence level by the P_{KH} -term. The model functions, but not with good quality, for transition in a separated layer under an elevated level of free-stream turbulence.

For modelling bypass transition in an attached boundary layer, the turbulent kinetic energy, k , is split into a small-scale part, k_s , and a large-scale part, k_l , by $k_s = f_{SS} k$ and $k_l = k - k_s$.

The shear-sheltering effect is expressed with the function f_{SS} , which contains three constants, C_S , C_χ and C_k . The function and the constants (see Table 1) are the same as in the model version by Kubacki and Dick (2016) (see also Kubacki et al., 2020). The f_{SS} -function is:

$$f_{SS} = \exp(-C_{SS}\nu/\sqrt{k}y)^2, \quad \text{with} \quad C_{SS} = C_S(1 + f_k\chi), \quad (3)$$

where χ and f_k are functions that express curvature effects and contain C_χ and C_k .

The shear-sheltering function models the damping of the small-scale turbulent fluctuations by the boundary layer shear. With $k_s = f_{SS}k$ and $k_l = k - k_s$, only the large-scale turbulent fluctuations, with energy k_l , penetrate to the vicinity of the wall in a laminar layer. The large-scale fluctuations physically generate the streaks. They do not produce turbulence directly, but only indirectly when the streaks cause breakdown. The small-scale fluctuations, with energy k_s , are restricted to the outer part of the layer. These contribute directly to the production of turbulent kinetic energy, which is expressed by the production terms $P_k = \nu_s S^2$. When the turbulence penetrates sufficiently close to the wall, the breakdown is simulated by activation of the intermittency function:

$$\gamma = \min\left(\max\left(\frac{\sqrt{k}y}{A_\gamma\nu} - 1, 0\right), 1\right). \quad (4)$$

The value of the constant A_γ (see Table 1) is the same as in the previous model version.

The small- and large-scale eddy viscosities are defined by:

$$\nu_s = \frac{k_s}{\tilde{\omega}_s}, \quad \text{with} \quad \tilde{\omega}_s = \max\left[\omega, C_{\text{lim}} \frac{S}{a_1}\right], \quad \nu_l = \frac{k_l}{\tilde{\omega}_l}, \quad \text{with} \quad \tilde{\omega}_l = \max\left[\omega, C_{\text{lim}} \frac{S}{a_2}\right]. \quad (5)$$

The effective eddy viscosity, used in the Navier-Stokes equations, is $\nu_T = \nu_s + \nu_l$. At walls, the standard conditions for k and ω are imposed (Wilcox, 2008): $k = 0$, $\omega = 6\nu/(\beta_0 y^2)$.

The P_{KH} -production term (Kelvin-Helmholtz) in Eq. (1) is

$$P_{KH} = C_{KH} F_{KH} \nu S^2, \quad \text{with} \quad F_{KH} = \min\left(\max\left(\frac{R_S}{2.2A_{KH}} - 1, 0\right), 1\right) \quad \text{and} \quad R_S = \frac{S y^2}{\nu}. \quad (6)$$

The production term P_{Kleb} (Klebanoff) in Eqs. (1) and (2) is

$$P_{Kleb} = C_{Kleb} f_{Kleb} k S. \quad (7)$$

The f_{Kleb} -function is a sensor for detection of the front part of a separated boundary layer, defined as the product of three functions:

$$f_{Kleb} = f_\gamma f_\omega f_w, \quad \text{with} \quad (8)$$

$$f_\gamma = \frac{1}{1 + \exp[b_\gamma(\gamma - a_\gamma)]}, \quad f_\omega = \frac{1}{1 + \exp[-b_\omega(\text{Re}_\omega - a_\omega)]}, \quad f_w = \exp\left[-\left(\frac{R_t}{c_w}\right)^2\right]. \quad (9)$$

The f_γ - and f_ω -functions are the same as used by Kubacki et al. (2020) in a first version of the current model. By the value $a_\gamma = 0.95$, the f_γ -function is zero in the outer zone of a laminar boundary layer, also a separated one, in the turbulent part of an attached turbulent boundary layer and in the free-stream. The $b_\gamma = 150$ determines the (strong) steepness of this function. The f_γ -function is near to unity close to a wall. The Reynolds number $\text{Re}_\omega = \omega y^2/\nu$ is about 85 in wall vicinity due to the wall

boundary condition of ω . By the value $a_\omega = 150$, the f_ω -function is near to unity away from a wall, outside an attached laminar boundary layer and outside the viscous sublayer of an attached turbulent boundary layer. The value $b_\omega = 5$ determines the steepness of this function. The f_ω -function is near to zero close to a wall. By the value $a_\omega = 150$, the f_ω -function reaches unity away from a wall, but still inside a separated laminar boundary layer, if this layer is sufficiently far away from the wall. This way, the product of the f_γ - and f_ω -functions becomes different from zero in the outer zone of a separated laminar boundary layer.

Additionally to the formulation in previous work (Kubacki et al., 2020), a small change is introduced to avoid spurious activity of the f_{Kleb} -function at the edge of an accelerating laminar boundary layer. This is done by multiplication by the wall-proximity function f_w in Eq. (8). The f_w -function is based on the turbulent Reynolds number, $R_t = k/(\omega \nu)$. The value of the c_w constant is set to 2.0. The f_w -function attains unity close to a wall and it evolves to zero approximately in the middle part of a boundary layer. The f_w -function thus keeps the activity zone of the sensor for boundary layer separation f_{Kleb} nearer to the wall than that of $f_{sep} = f_\gamma f_\omega$, used in previous work.

The major difference with respect to the previous extension of the originating model for coping with transition in separated state under elevated free-stream turbulence (Kubacki et al., 2020) is in the supplementary production term P_{Kleb} . In the previous version, a similar production term was made proportional to νS^2 , by analogy with the production term $\nu_s S^2$ for bypass transition. The resulting model functions quite well, provided that the expression of intermittency (Eq. 4) is also made dependent on the sensor function $f_{sep} = f_\gamma f_\omega$. The development of the model started before the construction of the correlation of the Reynolds stress tensor and the shear rate tensor in transitional flows (Lengani et al., 2020). With the obtained correlation, it is now possible to construct the supplementary term P_{Kleb} on a rational basis. The outcome is that the modification of the intermittency function (Eq. 4) is not necessary anymore. The resulting model is thus much simpler.

The P_{KH} and P_{Kleb} terms are boosting terms in the transport equations (1-2). In a separated laminar boundary layer, both the shear-sheltering function (Eq. 3) and the intermittency factor (Eq. 4) have very low values. The production terms based on P_k are thus very small. By activation of the boosting terms, a local increase of the turbulent kinetic energy is obtained, which, when sufficiently strong, activates the intermittency factor (Eq. 4), which then starts the main production terms based on P_k . Part of the modelling of transition in separated state is thus done with the same terms as for bypass transition in an attached boundary layer.

The functioning in a separated layer is that first P_{KH} is activated by a sufficiently high value of the shear Reynolds number R_S , thus shear far enough from a wall. The production by P_{KH} is proportional to νS^2 , thus independent of the turbulence level. It represents turbulence produced by breakdown due to the instability of the Kelvin-Helmholtz rolls. Under a strong adverse pressure gradient, the production of modelled turbulent kinetic energy by this term is not sufficient to realise fast enough reattachment of the separated layer. When the separation zone becomes sufficiently large, the P_{Kleb} term becomes active. The production by this term is proportional to $k S$. Therefore, it can express the faster breakdown caused by the streaks perturbing the Kelvin-Helmholtz rolls under elevated free-stream turbulence.

FUNCTIONING OF THE SENSOR FUNCTION F_{KLEB}

Figure 1 shows results for flow along a flat plate under a strong adverse pressure gradient and a moderately high free-stream turbulence level (Tu=1.5%). Contour plots of the mean velocity component in the plate direction and the f_{Kleb} -function are shown. There is a long separation bubble on the plate. As desired, the f_{Kleb} -function is mostly active in the front part of the separation bubble.

FORMULATION OF THE BOOSTING SOURCE TERM P_{KLEB}

The P_{Kleb} by Eq. (7) is derived from the elastic-net regression model for the Reynolds stresses in transitional flows by Lengani et al. (2020).

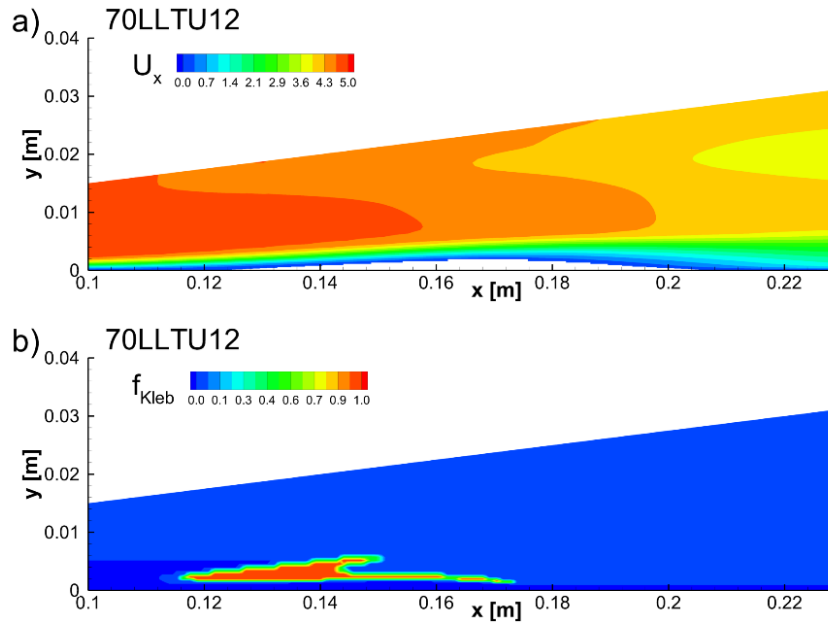


Figure 1: 70LLTU12 case (moderately high turbulence level and strong APG). Contour plots of a) mean x-velocity component and b) f_{Kleb} -function for simulation of separation-induced transition with the present model. The x-velocity is negative in the blanked zone in panel (a).

In that work, the Reynolds stress tensor $\overline{u'_i u'_j}$ is written as $\frac{2}{3}k(\delta_{ij} + \tau_{ij})$, with δ_{ij} the unit tensor and τ_{ij} the nondimensional deviatoric stress tensor. The nondimensional tensor τ_{ij} is symmetric and has zero trace. It may thus be written as $\tau_{ij} = X_\tau \Lambda_\tau X_\tau^T$, with X_τ its nondimensional eigenvector matrix and Λ_τ its nondimensional eigenvalue matrix. The shear rate tensor S_{ij} is also symmetric and has zero trace. Similarly to τ_{ij} , it may be written as $S_{ij} = X_S \Lambda_S X_S^T$, with X_S its nondimensional eigenvector matrix and Λ_S its dimensional eigenvalue matrix.

In a mean 2D flow, the expressions are:

$$\Lambda_\tau = \begin{bmatrix} \lambda_\tau & 0 \\ 0 & -\lambda_\tau \end{bmatrix}, \quad \Lambda_S = \begin{bmatrix} S & 0 \\ 0 & -S \end{bmatrix}, \quad X_S = \begin{bmatrix} \cos(\theta_S) & -\sin(\theta_S) \\ \sin(\theta_S) & \cos(\theta_S) \end{bmatrix}, \quad X_\tau = \begin{bmatrix} \cos(\theta_\tau) & -\sin(\theta_\tau) \\ \sin(\theta_\tau) & \cos(\theta_\tau) \end{bmatrix}.$$

The θ -angles express the orientation of the first eigenvectors.

Both tensors are obtained by:

$$\begin{bmatrix} S_{ij} \end{bmatrix} \quad \text{or} \quad \begin{bmatrix} \tau_{ij} \end{bmatrix} = X \begin{bmatrix} \lambda & 0 \\ 0 & -\lambda \end{bmatrix} X^T = \lambda \begin{bmatrix} \cos(2\theta) & \sin(2\theta) \\ \sin(2\theta) & -\cos(2\theta) \end{bmatrix}.$$

With $\Delta\theta = \theta_\tau - \theta_S$, the τ_{ij} -matrix can be written as:

$$\begin{bmatrix} \tau_{ij} \end{bmatrix} = \lambda_\tau \begin{bmatrix} \cos(2\theta_S + 2\Delta\theta) & \sin(2\theta_S + 2\Delta\theta) \\ \sin(2\theta_S + 2\Delta\theta) & -\cos(2\theta_S + 2\Delta\theta) \end{bmatrix}. \quad (10)$$

The angle θ_S is determined by the velocity field. Representation of the Reynolds stress tensor thus requires expressions for λ_τ and $\Delta\theta$. The production term P_k in the k - and ω - equations is: $-\frac{2}{3}k(\delta_{ij} + \tau_{ij})S_{ij} = -\frac{2}{3}k\tau_{ij}S_{ij}$. The result with the expression (10) is:

$$\begin{aligned}
P_k &= -\frac{2}{3} k \tau_{ij} S_{ij} = -\frac{2}{3} k \lambda_\tau S [2 \cos(2\theta_\tau) \cos(2\theta_S) + 2 \sin(2\theta_\tau) \sin(2\theta_S)] \\
&= -\frac{2}{3} k \lambda_\tau S \cos(2\Delta\theta) = \frac{2}{3} k \lambda_\tau S [-\cos(2\Delta\theta)].
\end{aligned} \tag{11}$$

Correlations for λ_τ and $\Delta\theta$ have been constructed as polynomial expansions of a Reynolds number, a non-dimensional representation of S and a non-dimensional representation of k . The basic term for λ_τ is about 0.557 and for $-\Delta\theta$ about 1 radian. With these values, the production term (11) becomes: $P_k = 0.155 k S$. Therefore, we express P_{Kleb} by Eq. (7) with $C_{Kleb} = 0.155$, without any further tuning. We do not take higher-order terms in the expansions of λ_τ and $\Delta\theta$ into account. This is technically possible and we tested the use of the expressions (results are not shown here). The correlations are valid for a large range of transitional flows, but we only need these in the limited area defined by f_{Kleb} . Because the P_{Kleb} -term is only used in a limited area, the higher-order terms have almost no effect.

Table 1. Transition model constants.

| Bypass transition | | | | | | | |
|-------------------------------|----------|------------|------------|------------|------------|------------|-------|
| A_γ | C_S | C_χ | C_k | a_1 | a_2 | | |
| 12.0 | 21.0 | 10.0 | 6.0 | 0.30 | 0.60 | | |
| Separation-induced transition | | | | | | | |
| C_{KH} | A_{KH} | C_{Kleb} | a_ω | b_ω | a_γ | b_γ | c_w |
| 2 | 550 | 0.155 | 150 | 5 | 0.95 | 150 | 2 |

RESULTS OF UNIGE FLAT PLATE CASES

The quality of the P_{Kleb} -term (Eq.7) for transition in a separated boundary layer is illustrated by simulation of four flows over a flat plate from the data base by Simoni et al. (2019). The selected cases (Table 2) are with transition in a separated boundary layer subjected to a strong (70LTU12) and a moderate (70HTU9) adverse pressure gradient, bypass transition in an attached boundary layer (220LTU5), and a flow without transition along the plate (150LLTU5). The cases are part of the 48 cases (called UNIGE) used by Lengani et al. (2020) for the elastic-net regression. The four cases presented were used for tuning of the model constants. We tested the model performance on other flows from the same data base, but these results are not shown here.

Table 2. Selected UNIGE cases. The Reynolds number is based on the plate length and the mean free-stream velocity at the leading edge of the plate. The turbulence intensity, Tu, is defined at the boundary layer edge at the inlet to the computational domain (60 mm downstream of the leading edge of the plate).

| Test case | Re | Tu [%] | Pressure gradient | Transition mode / flow |
|-----------|--------|--------|-------------------|------------------------|
| 70LTU12 | 70000 | 2.5 | strong APG | separation-induced |
| 70HTU9 | 70000 | 3.5 | moderate APG | separation-induced |
| 220LTU5 | 220000 | 2.5 | low APG | bypass |
| 150LLTU5 | 150000 | 1.5 | low APG | no transition/laminar |

The flow domain of the measurements by Simoni et al. (2019) is trapezoidal, as shown in Fig. 2. The boundaries are the AB, BC and CD sides. The height of the AB and CD sides is 10 and 40 mm,

respectively. The BC side starts at 10 mm above the plate at 60 mm downstream the leading edge and ends at 40 mm above the plate at the streamwise distance of 300 mm. The AB and BC sides are inflow boundaries with imposed values of the mean velocity components and the turbulent quantities k and ω . Determination of the turbulent kinetic energy on the boundary AB requires splitting of measured fluctuations into turbulent and coherent parts. The splitting was done with the procedure described by Simoni et al. (2019). The CD boundary is an outflow boundary with imposed pressure and zero normal flux conditions for the velocity components and the turbulent quantities. Standard no-slip conditions were specified along the plate.

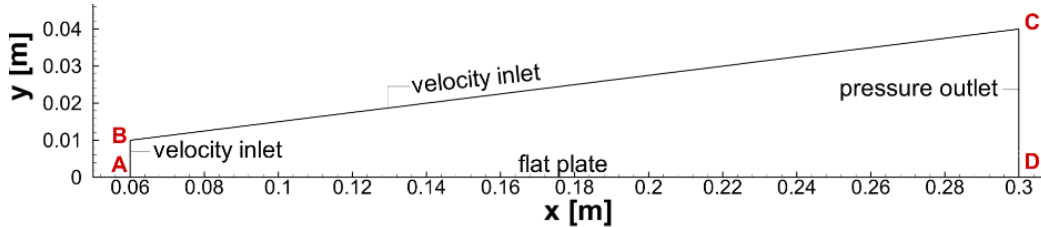


Figure 2: UNIGE flat plate (Simoni et al. 2019). Computational domain (bounded by AB, BC, CD sides) and boundary conditions. The AB and BC sides are inlets on which LDV data of mean velocity components and turbulent quantities are available. Flow is from left to right.

Steady 2D incompressible Navier-Stokes equations were employed. The convective terms in the momentum and the transport equations were discretised with the second-order upwind scheme and the diffusive terms with the central scheme, available in the ANSYS Fluent CFD-package (version 18.2). The transition model was implemented by the UDF-functionality. The solution of the RANS-equations was obtained with the coupled pressure-based algorithm with iterations done until the normalised residuals of the momentum and the transport equations were reduced below 10^{-6} .

A hybrid grid was generated with a structured part near the plate and an unstructured part away from the plate. The total number of cells was 36000. The nondimensional distance y^+ was below 0.01 along the plate. A grid sensitivity study was performed with a coarser grid with 25000 cells (y^+ about 1 along the plate) and a finer grid with 77000 cells, obtained by refining the unstructured part (y^+ below 0.01). The grid independence of the results was verified by inspection of the shape factor profiles along the plate (not shown). No essential differences were observed between the results on the three grids. Therefore, the basic grid with 36000 cells was selected for the final study.

Figure 3 presents measured and computed mean velocity components and turbulent kinetic energy at the distance $y/L=0.04$ above the plate, for the 150LLTU5 and 220LTU5 cases. The bars indicate uncertainty bounds: relative error 3% on mean velocity components and relative error 6 to 10% on rms of fluctuating velocity components. The agreement between measurements and simulations is good. The agreement is similar for the two other cases (not shown). It means that proper inlet values of flow variables and modelled scalars are specified along the AB and BC sides.

Figure 4 shows the evolution of the shape factor along the plate obtained with the previous version (Kubacki and Dick, 2016b) and the current modified version of the algebraic transition model. The comparison is made with measurements by Simoni et al. (2019). The uncertainty in the measured shape factor is shown by error bars (6 to 10%). Both models produce results with similar quality for the cases without transition along the plate (Fig. 4 a) and with bypass transition (Fig. 4 b).

The modified model produces results with much better quality for the cases with separation-induced transition (Fig. 4 c and d). The extension of the separation bubble and the position of the maximum shape factor are well predicted for the cases with separated-flow transition (70LTU12, 70HTU9). But the maximum value of the predicted shape factor is lower than the experimental value. This is caused by the way of modelling the transition, which is not entirely physically correct. The transition in separated state is modelled by production of turbulent quantities k and ω by the terms P_{KH} and P_{Kleb} . In reality, perturbations by Kelvin-Helmholtz instability and by Klebanoff streaks are initially coherent and only produce turbulence at the breakdown of the coherent flow. The fluctuations

are thus initially of laminar type. By the current modelling, without description of laminar fluctuation kinetic energy, the initial fluctuations are represented as turbulent. Taking into account this inherent feature of the modelling, the results prove that the P_{Kleb} -term (Eq. 7) functions well for modelling the effects of the Klebanoff streaks on the separated boundary layer.

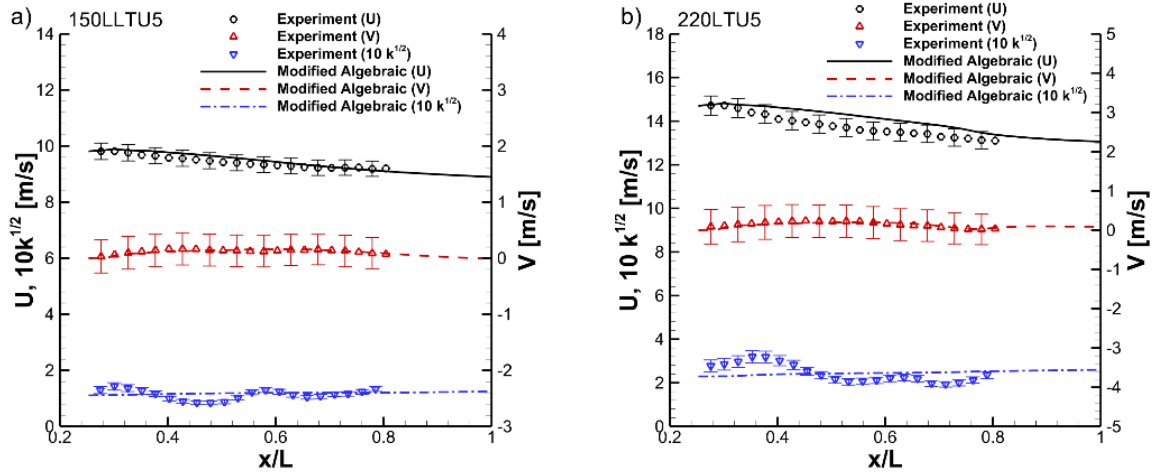


Figure 3: UNIGE flat plate. Mean x- and y-velocity components and turbulent kinetic energy, k , along $y/L=0.04$ for a) 150LLTU5 and b) 220LTU5 cases. Symbols denote the PIV results by Simoni et al. (2019). The bars indicate the uncertainty bounds of the experimental data.

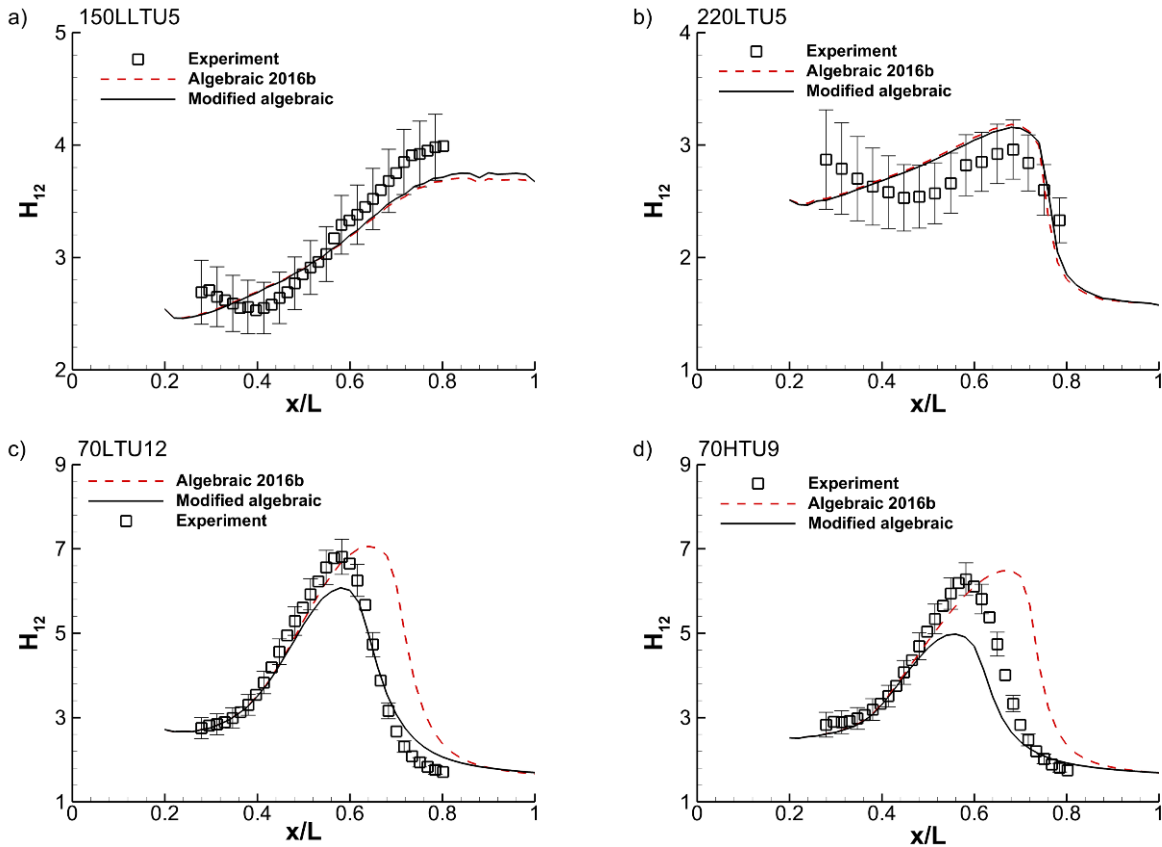


Figure 4: UNIGE flat plates. Shape factor evolutions on the plate for a) 150LLTU5 case (laminar boundary layer), b) 220LTU5 case (bypass transition), c) 70LTU12 and d) 70HTU9 cases (separation-induced transition). The bars indicate the uncertainty bounds of the experimental data.

RESULTS OF PREVIOUSLY USED CASES

It is essential that the modification by the P_{Kleb} -term (Eq.7) does not deteriorate the results of the tuning cases of the previous model version. Verification is presented here on some cases used in previous work: two ERCOFTAC T3C flat plate cases and the two flows over the N3-60 steam-turbine vane cascade, experimentally studied by Zarzycki and Elsner (2005). The computational grids consist of 0.8×10^5 and 1.1×10^5 cells for the T3C and N3-60 cases, respectively. We refer to Kubacki and Dick (2016) for the discussion of grid-independence study, numerical schemes and solver settings. Table 3 lists the inlet values of the mean and turbulent flow variables. The modified model produces identical evolutions of the free-stream turbulence levels as in previous work (not shown).

Figure 5 shows the skin friction on the flat plate for the T3C cases. In these cases, bypass transition takes place inside the attached boundary layer. The transition onset is well predicted by both model versions, but the transition length is too short with respect to reality. The too rapid transition is due to the algebraic description of the intermittency. Once transition is triggered by activation of the intermittency function (Eq. 4), the intermittency grows rapidly towards the wall. The asymptotic behaviour in the turbulent region, at large distance from the leading edge is better with the modified model. This is not caused by the P_{Kleb} -term in Eqs. (1) and (2), but results from modification of the a_2 constant in Eq. (5) from 0.45 to 0.6, as discussed in Kubacki et al. (2020).

Table 3. Boundary conditions at the inlet of the computational domain and free-stream turbulence intensity in the leading edge plane for the ERCOFTAC flat plates and the N3-60 cascade. U denotes the velocity normal to the inlet boundary.

| Test case | U [m/s] | Tu [%] | l_t [mm] | Tu_{LE} [%] |
|-------------------|-----------|------------|------------|---------------|
| T3C5 | 8.95 | ~ 3.0 | 7.0 | 3.0 |
| T3C3 | 3.85 | ~ 3.0 | 9.8 | 3.0 |
| N3-60, $Tu=0.4\%$ | 8.20 | ~ 0.4 | 2.0 | 0.4 |
| N3-60, $Tu=3.0\%$ | 8.20 | ~ 3.0 | 9.0 | 3.0 |

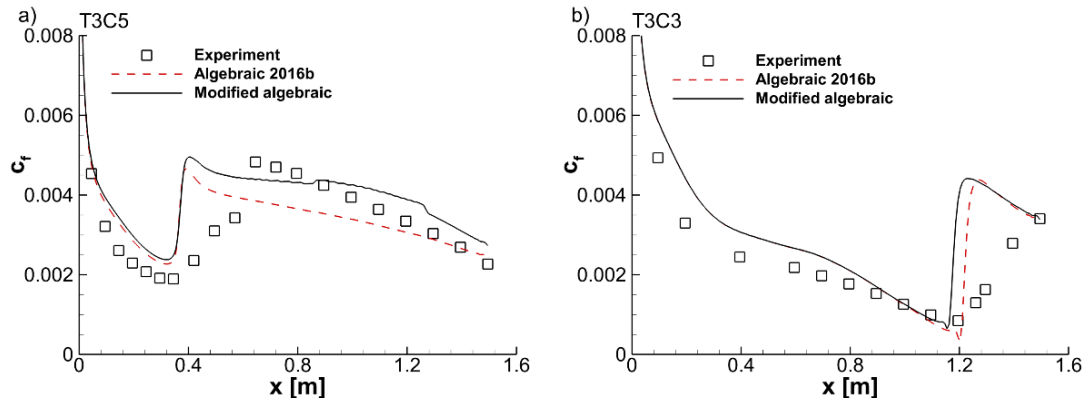


Figure 5: ERCOFTAC flat plates with variable streamwise pressure gradient. Skin friction coefficient on the plate surface for T3C5 and T3C3 cases.

Figure 6 shows the shape factor on the suction-side of the N3-60 blade at low ($Tu=0.4\%$) and high ($Tu=3\%$) free-stream turbulence levels. With the low free-stream turbulence level (Fig. 6 a), the transition is by Kelvin-Helmholtz instability in the separated shear layer near to the trailing edge of the blade. The transition is started with the P_{KH} -term and the P_{Kleb} -term is not active. The results by the previous model and the modified model are identical and agree very well with the experiment. With the high free-stream turbulence level (Fig. 6 b), bypass transition is triggered in the attached laminar boundary layer. Also in this case, the previous model and the extended model produce identical and good results.

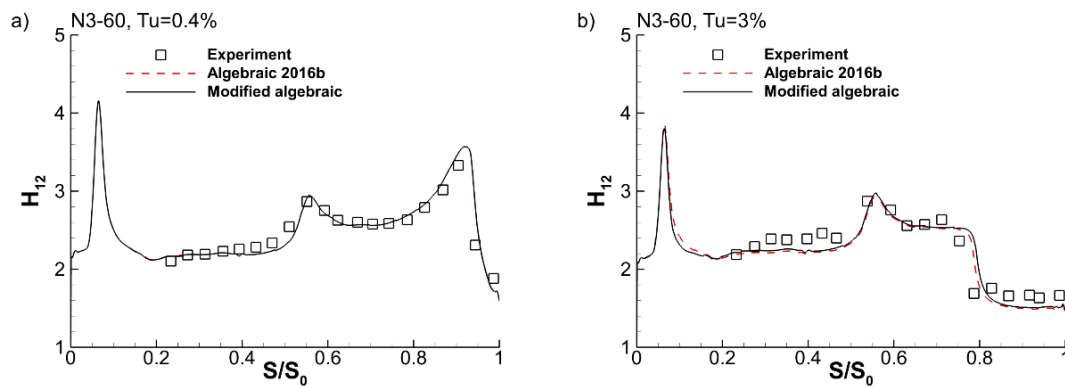


Figure 6: N3-60 turbine cascade. Shape factor on suction side of the blade for the free-stream turbulence level at the leading edge of the blade equal to a) $Tu=0.4\%$ and b) $Tu=3\%$.

CONCLUSIONS

The elastic-net regression model for Reynolds stresses in transitional flows by Lengani et al. (2020) has been incorporated into an algebraic intermittency model by a production term in the k - and ω - equations. The production term is activated by a sensor function detecting the front part of a separated boundary layer. The extended model does not alter the good results of the previous model for bypass transition and for transition in a separated boundary layer under a low free-stream turbulence level. The modified model improves the predictions of the previous model for transition in a separated boundary layer subjected to an elevated turbulence level combined with a moderate or high adverse pressure gradient.

ACKNOWLEDGEMENT

The first author acknowledges financial support from a research project funded by the Polish National Science Centre (Contract number DEC-2018/31/B/ST8/01717).

REFERENCES

- ERCOFTAC Data base of Transition Modelling Test Cases. Available online: <http://cfm.mace.manchester.ac.uk/ercoftac/>.
- Hosseinvardi, S., Fasel, H.F., (2019). *Numerical investigation of laminar-turbulent transition in laminar separation bubbles: the effect of free-stream turbulence*. J. Fluid Mech., 858, 714-759.
- Jacobs, R.G., Durbin P.A., (2001). *Simulations of bypass transition*. J. Fluid Mech., 428, 185-212.
- Kubacki, S., Dick, E., (2016). *An algebraic intermittency model for bypass, separation-induced and wake-induced transition*. Int. J. Heat Fluid Flow, 62, 344-361.
- Kubacki, S., Simoni, D., Lengani, D., Dick, E., (2020). *An extended version of an algebraic intermittency model for prediction of separation-induced transition at elevated free-stream turbulence level*. Int. J. Turbomach. Propuls. Power, 5, 28.
- Lengani, D., Simoni, D., Kubacki, S., Dick, E., (2020). *Analysis and modelling of the relation between the shear rate and Reynolds stress tensors in transitional boundary layers*. Int. J. Heat Fluid Flow, 84, 108615.
- McAuliffe, B.R., Yaras, M.I., (2010). *Transition mechanisms in separation bubbles under low- and elevated freestream turbulence*. J. Turbomach., 132, 011004.
- Simoni, D., Lengani, D., Dellacasagrande, M., Kubacki, S., Dick, E., (2019). *An accurate data base on laminar-to-turbulent transition in variable pressure gradient flows*, Int. J. Heat Fluid Flow, 77, 84-97.
- Wilcox, D.C., (2008). *Formulation of the k - ω turbulence model revisited*, AIAA J., 46, 2823-2838.
- Zarzycki, R., Elsner, W., (2005). *The effect of wake parameters on the transitional boundary layer on a turbine blade*. IMechE Part A, J. Power and Energy, 219, 471-480.